Supporting Information

A Functional Separator Enabling Safe and High-performance Sodium Metal Batteries under Elevated Temperature

Delong Yin [a], Tianyu Wei [a], Jia Guo [a], Kai Yang [a], Peng Chen [a], Hui Dou [ab*], Xiaogang Zhang [ab*]

[a]*Jiangsu Key Laboratory of Electrochemical Energy Storage Technologies, College of Materials Science and Technology, Nanjing University of Aeronautics and Astronautics, Nanjing 210016, China.*

[b]*National Key Laboratory of Mechanics and Control for Aerospace Structures, Institute for Frontier Science, Nanjing University of Aeronautics and Astronautics, Nanjing 210016, P.R. China.*

E-mail: Hui Dou: dh_msc@nuaa.edu.cn; Xiaogang Zhang: azhangxg@nuaa.edu.cn

1 Experimental Section

1.1 Synthesis of $Na_3Zr_2Si_2PO_{12}$-UiO-66-SO_3Na (N-Us)

The commercial NZSP particles, $ZrCl_4$ and 2-(sodiosulfo)terephthalic acid were dispersed in a mixed solution of acetic acid and DMF. The material ratio was based on a molar ratio of 3:1 for Zr atoms in NZSP to $ZrCl_4$, with both $ZrCl_4$ and 2-(sodiosulfo)terephthalic acid used at a molar ratio of 1:0.8. After one hour of ultrasonication and stirring, the dispersion was transferred to a hydrothermal autoclave and then reacted at 145 °C for 12 h. Following centrifugation and solvent exchange, the product was dried at 60 °C to obtain N-Us powder.

1.2 Synthesis of N-Us@PI

N-Us and PVDF were mixed at a mass ratio of 4:1 and dispersed in a DMF solvent to prepare a coating slurry. Subsequently, the dispersion was coated onto one side of a PI separator using a 10 μm doctor blade. After drying in a vacuum oven at 60 °C for 6 h, the N-Us@PI composite separator was obtained. The composite separator was then cut into circular pieces with a diameter of 1.9 cm for use in button cells and other tests, as well as into rectangular separators measuring 7 cm × 9 cm for the assembly of pouch cells.

1.3 Material characterizations

Fourier-transform infrared spectroscopy (FTIR, Bruker INVENIO-R) was used to detect the functional groups on the surface of N-U particles. The crystal structure was determined by X-ray diffraction (XRD, Empyrean). X-ray photoelectron spectroscopy (XPS, ESCALAB Xi+) was used to detect the change of chemical bonds on the surface of N-U particles and the change of chemical composition on the surface of subsequent separators. Morphology and micro-structure of N-Us@PI separator was characterized by SEM (LYRA3 GMU) and TEM (Talos F200X G2). Elements composition of N-Us@PI separator had been qualitatively analyzed by scanning electron microscope EDS spectrometer. Atomic Force Microscope (AFM, SPM9700-HT) was applied to analyze the roughness of separator and young's modulus. The surface area value and pore size of the composite separator was characterized using automated surface area

and porosity analyzer (BET, ASAP 2460).

1.4 Electrochemical measurements

To check the wettability of the separators to the liquid electrolyte, the separators were immersed in 2 mL of liquid electrolyte (1.0 M $NaClO_4$ in EC: DEC = 1:1 v/v, with 5% FEC) for 5 minutes. Prior to weighing the infiltrated separator, it is necessary to remove any excess electrolyte adhering to the surface due to surface tension and related effects. Furthermore, the electrolyte uptake, U (%), was calculated by weighing the separator before (W_0) and after complete absorption of the liquid electrolyte (W), as shown in equation (1):

$$U(\%) = \frac{W - W_0}{W_0} \times 100\% \quad (1)$$

The porosity of the separator was tested by infiltrating the composite separator in n-butanol solvent for 5 minutes. Prior to weighing the infiltrated separator, it is necessary to remove any excess solvent adhering to the surface due to surface tension and other factors, ensuring that the calculated volume corresponds to the entire separator. The porosity was obtained by the following equation (2):

$$P(\%) = \frac{M - M_0}{\rho V} \times 100\% \quad (2)$$

where P (%) is the porosity of the separator, M_0 represents the initial quality, M represents the quality after infiltration, ρ represents the density of n-butanol and V represents the volume of separator.

The ionic conductivity of separators was performed by sandwiching the electrolyte-soaked separator between two steel plates. EIS was determined with constant perturbation amplitude of 10 mV in the frequency range from 100 mHz to 5 MHz. The ionic conductivity was calculated using the EIS, as shown in equation (3):

$$\sigma = \frac{L}{B \times S} \quad (3)$$

where σ is the ionic conductivity, L represents the thickness of the separator, B is the bulk resistance, and S is the area of the steel plate.

The Na^+ transference number was ascertained through a combination of

chronoamperometry and EIS analyses on the symmetrical Na||separator||Na cells. The chronoamperometry profile was obtained at a potential difference of 10 mV for 3600 s and the AC impedance spectra were tested before and after polarization. The Na^+ transference number was obtained by the following equation (4):

$$t_{Na+} = \frac{I_{SS}\,(\Delta V - I_0 R_0)}{I_0\,(\Delta V - I_{ss} R_{ss})} \quad (4)$$

where t_{Na+} represents the transference number of Na^+, I_0 and I_{ss} are the initial and stable current (mA), R_0 and R_{ss} are the resistance before and after potentiostatic polarization (Ω), and V stands for the potentiostatic voltage (V).

The desolvation energy of Na^+ was derived by fitting the charge-transfer resistances measured at different temperatures using the Arrhenius equation, as shown in equation (5):

$$1/R_{ct} = Aexp(-\frac{E_a}{RT}) \quad (5)$$

Where A is the pre-exponential factor, R is the gas constant, and T is the temperature (k).

NVP, conductive carbon black and PVDF were added to an appropriate volume of N-methylpyrrolidone solution with mass ratio of 8:1:1 and ball milled for 3 h to obtain the homogeneous cathode slurry. After that, the homogeneous slurry was casted on an aluminum foil by a doctor blade. After drying at 110 °C for 1 h and vacuum drying at 110 °C for 12 h. The NVP loadings are about 3 mg cm^{-2}. All cells were assembled with a CR2025 coin cell in an Ar-filled glovebox (H_2O < 0.1 ppm, O_2 < 0.1 ppm). All electrochemical tests were performed using the Neware cell system (China) at a temperature of 25 °C. The electrolyte is 1.0 M $NaClO_4$ in EC:DEC = 1:1 v/v, with 5% FEC.

During the NVP||Na full cells assembly, Na metal was used as anodes. PI and N-Us@PI were employed as separators for comparison. 60 μL of ester-electrolyte was injected into the full cells. The pouch cell was configured as follows: The cathode consisted of a low-loading NVP electrode with dimensions of 5 × 5 cm and a mass loading of 3 mg cm^{-2}, while the anode was a metallic sodium sheet measuring 5 × 5 cm with a thickness

of 300 μm. The total amount of electrolyte injected was 1.5 mL. In addition, all cells were pre-cycled for activation at a rate of 0.1 C for three cycle, and capacity retention was calculated starting for the fourth cycle. The electrochemical performance of the full cells was measured between 2.0 ~ 4.0 V.

1.5 Computational methods

Density-functional theory (DFT) simulation calculation: The mechanism of action of SO_3^- groups on the surface of N-Us particles on anions was analysed by DFT. The energy cutoff was set to 450 eV. Brillouin-zone integrals were sampled using a 2 × 2 × 1 Γ-centered Monkhorst-Pack mesh, and the structure was fully relaxed until the maximum force on each atom was lower than 0.03 eV/Å, with an energy convergence criterion of 10^{-5} eV. The charge density difference was expressed as Δρ=ρ_(*M)-ρ_*-ρ_M, where ρ_(*M), ρ_*, and ρ_M are the electron densities of the isolated surface, isolated M molecule, and surface including the adsorbed M molecule, respectively, The adsorption energy Eads was defined as E_ads=E_(*M)-E_*-E_M, where E_(*M) stands for the energy of the monolayer with the adsorbed M molecule, E_* is the energy of the isolated surface, and E_M is the energy of an isolated M molecule in vacuum. We performed spin-polarized DFT calculations using the Vienna ab initio.

2 Supporting Figures

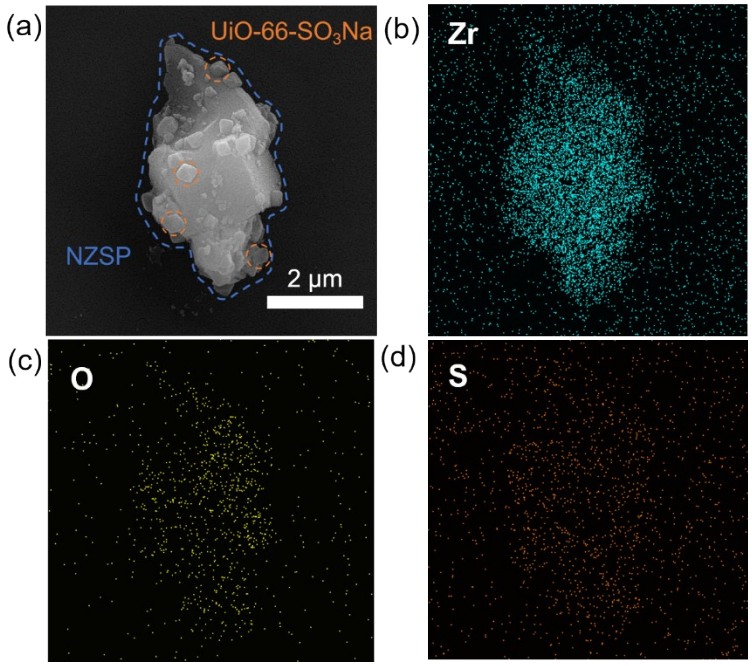

Fig. S1. (a) SEM image of N-Us particles and the elemental distribution of (b) Zr, (c) O, and (d) S.

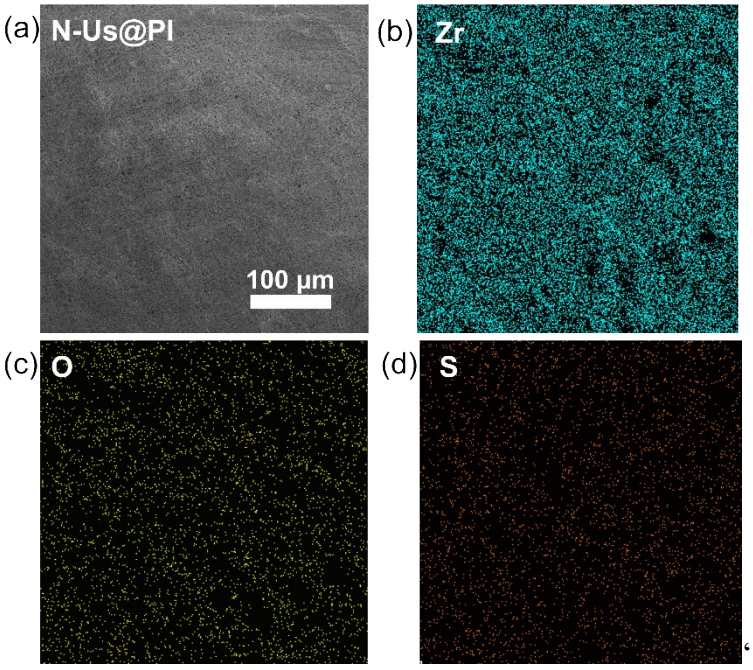

Fig. S2. Surface characterization of the N-Us@PI separator: (a) SEM image and elemental distribution maps of (b) Zr, (c) O, and (d) S.

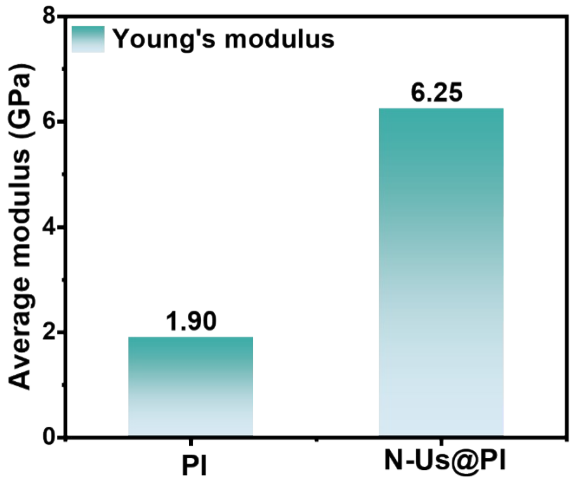

Fig. S3. The surface Young's modulus of PI and N-Us@PI separators.

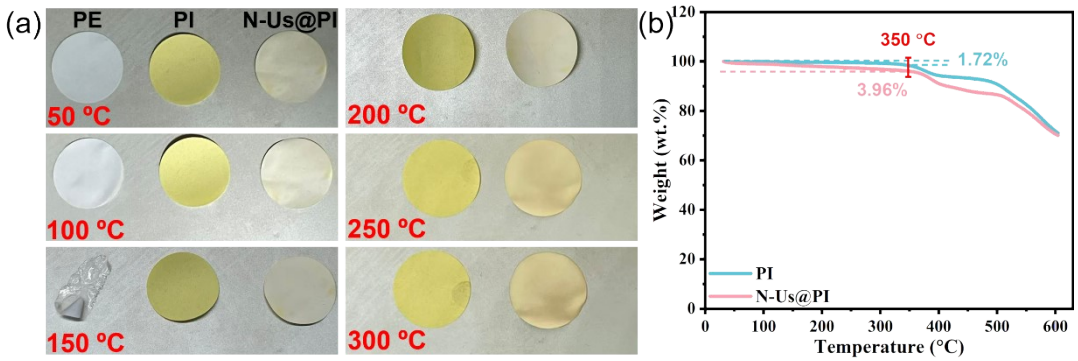

Fig. S4. (a) Images of PE, PI, and N-Us@PI separators at various temperatures, (b) the TGA curves of PI and N-Us@PI separators.

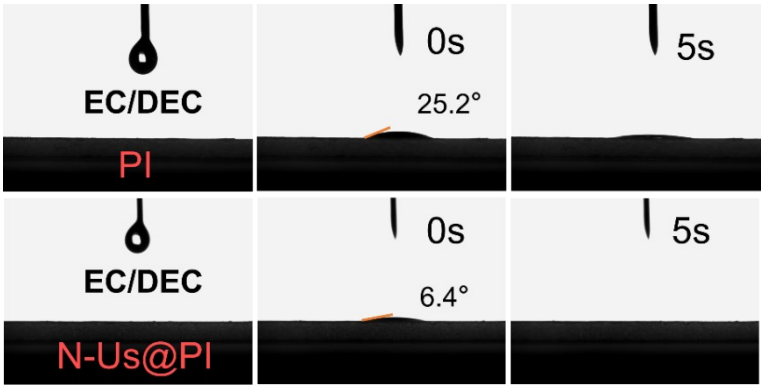

Fig. S5. Contact angles of PI and N-Us@PI separators with carbonate electrolyte solutions

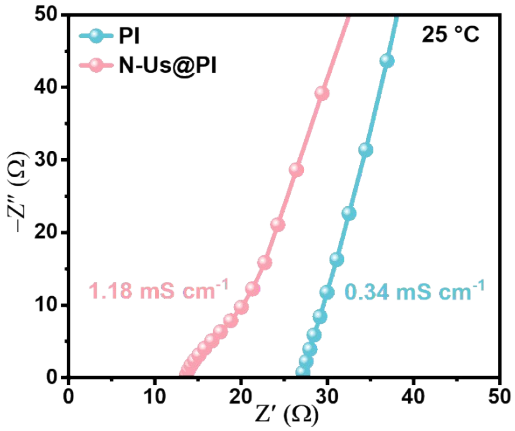

Fig. S6. The ionic conductivitis of PI and N-Us@PI separators at 25 °C.

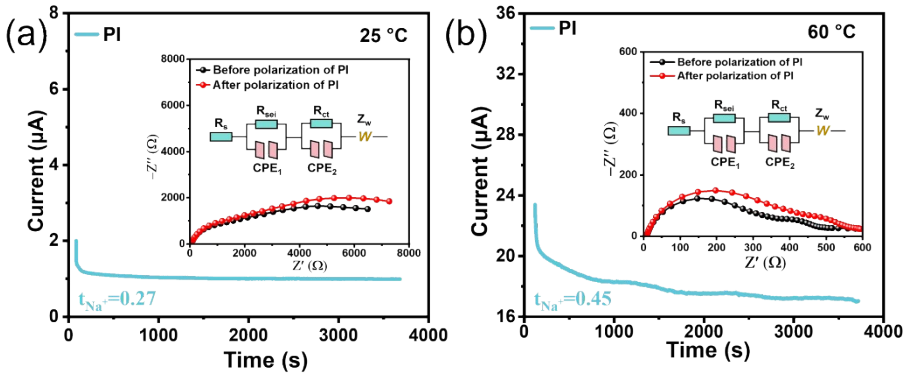

Fig. S7. Na^+ transference numbers of PI separators at different temperatures: (a) 25 °C, (b) 60 °C.

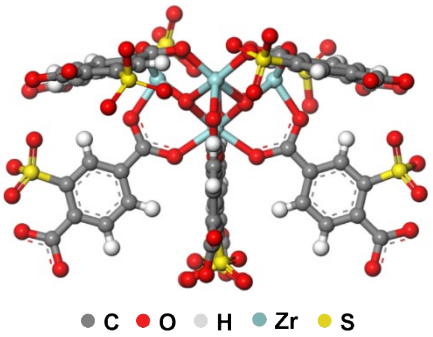

Fig. S8. Schematic diagram of UiO-SO_3^-.

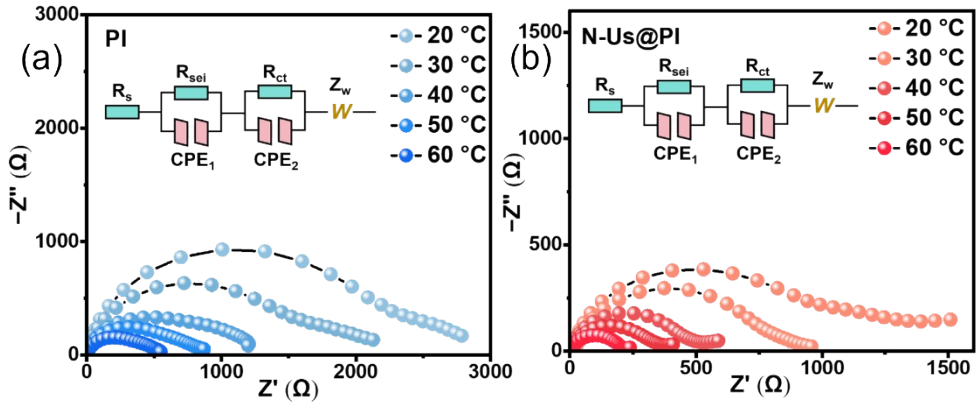

Fig. S9. EIS of Na||Na symmetric cells employing different separators at various temperatures: (a) Na|PI|Na, and (b) Na|N-Us@PI|Na.

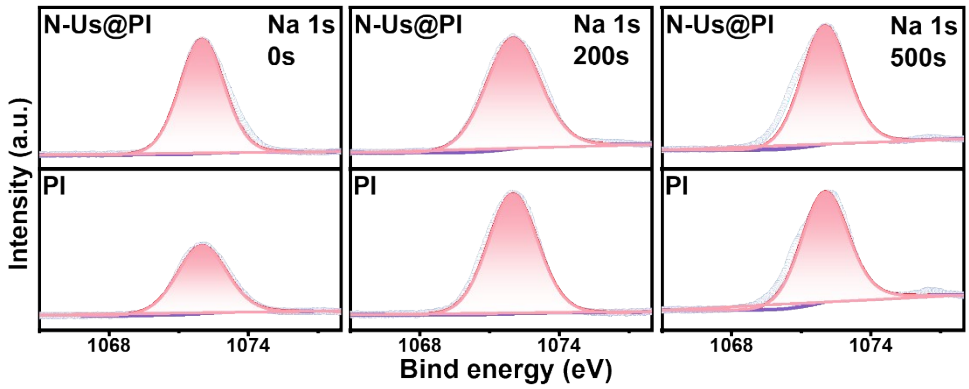

Fig. S10. Na 1s XPS spectra of Na anode after 20 cycles at 25 °C for different etching times.

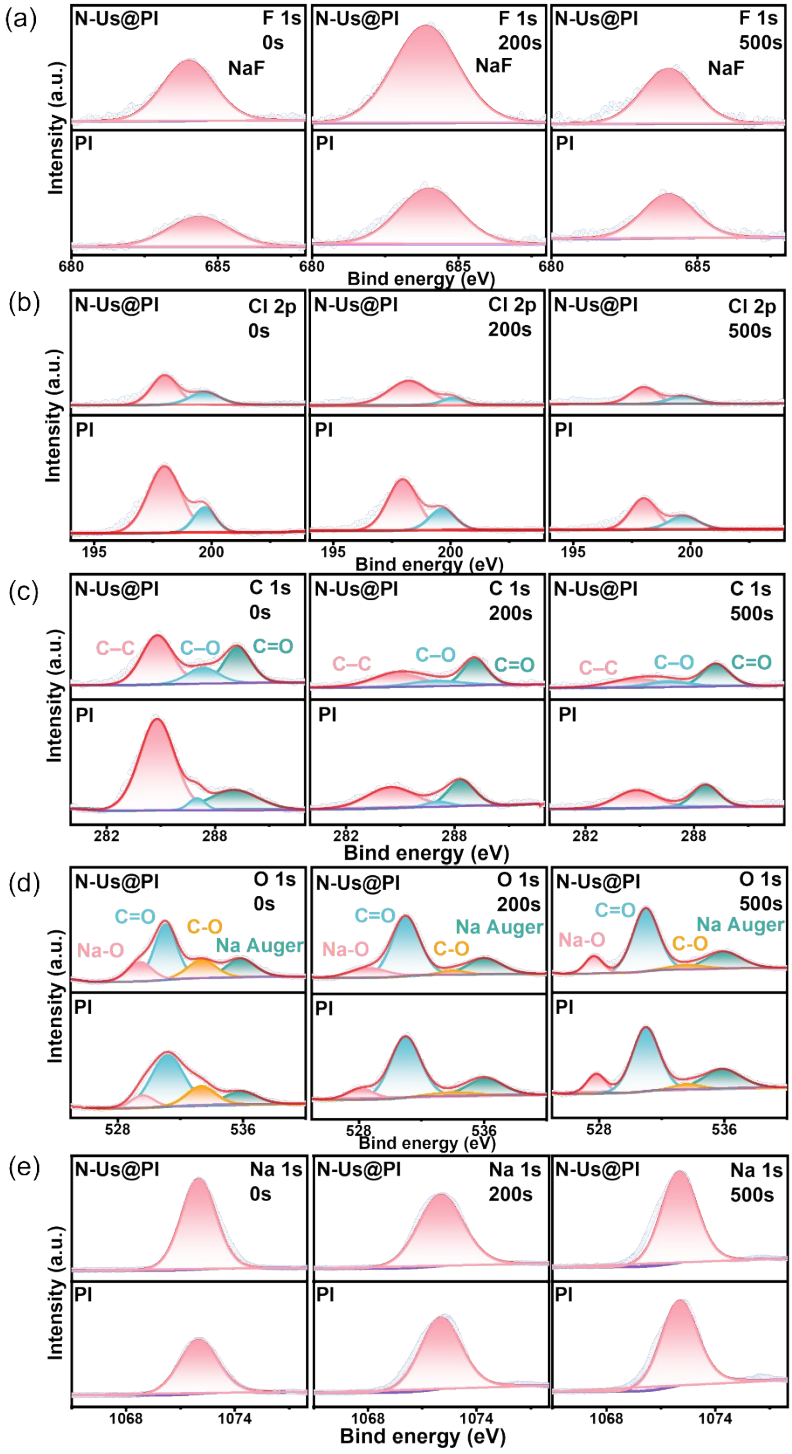

Fig. S11. (a) F 1s, (b) Cl 2p, (c) C 1s, (d) O 1s, and (e) Na 1s XPS spectra of Na anode after 20 cycles at 60 °C for different etching times.

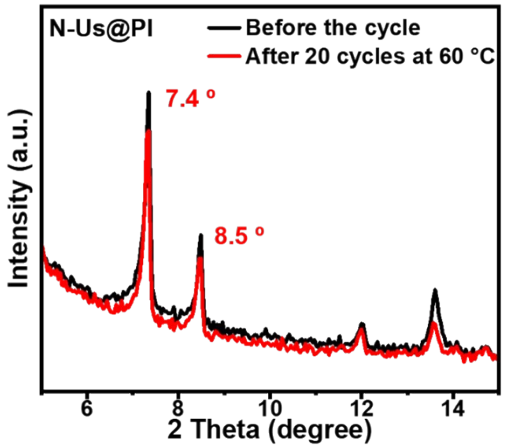

Fig. S12. XRD of the N-Us@PI separator before and after 20 cycles in a Na||Na symmetric cell.

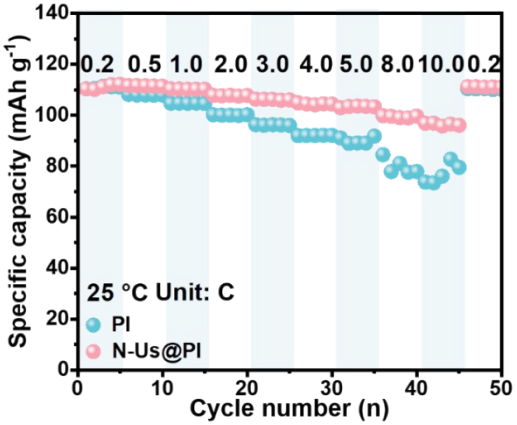

Fig. S13. Rate capability of Na||NVP batteries employing different separators.

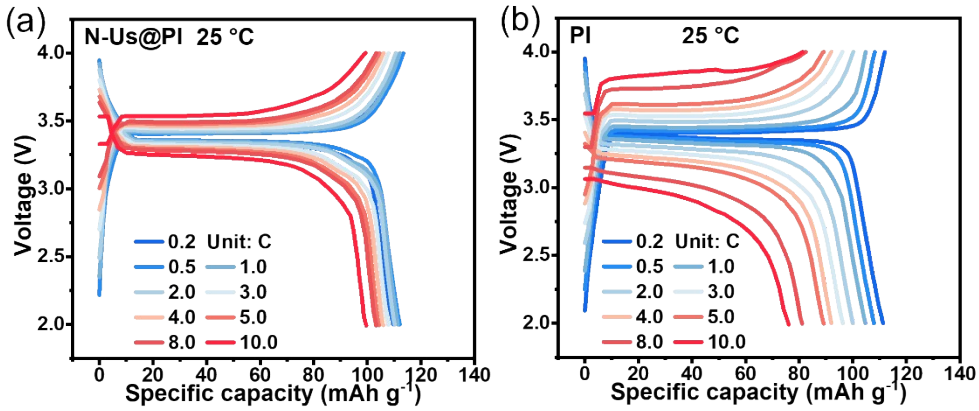

Fig. S14. GCD of Na||NVP batteries employing different separators at 25 °C under various current rates: (a) Na|N-Us@PI|NVP, and (b) Na|PI|NVP.

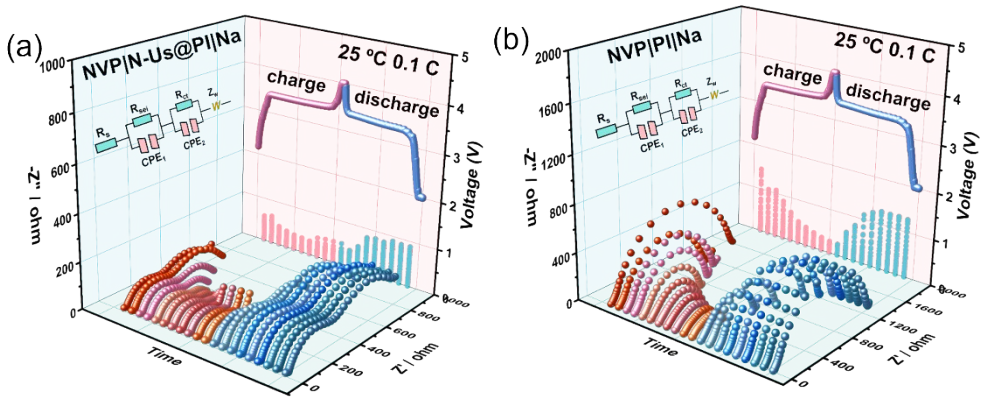

Fig. S15. *In-situ* EIS of Na||NVP batteries employing different separators at 25 °C and 0.1 C: (a) Na|N-Us@PI|NVP, and (b) Na|PI|NVP.

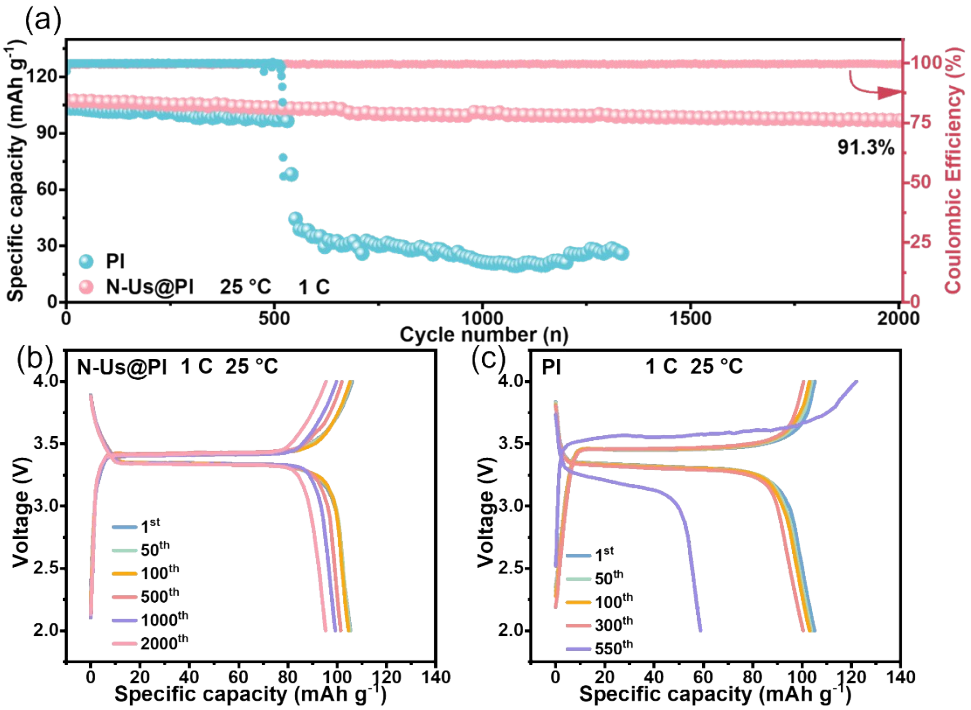

Fig. S16. The cycling stability Na||NVP batteries employing different separators at 25 °C and 1 C: (a) Cycle performance; GCD profiles of (b) Na|N-Us@PI|NVP and (c) Na|PI|NVP.

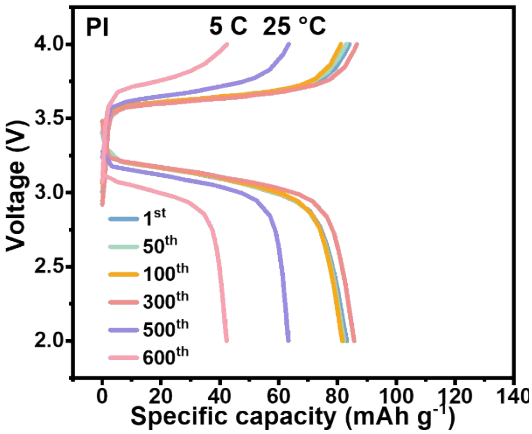

Fig. S17. GCD profiles of Na|PI|NVP batteries at 25 °C and 5 C.

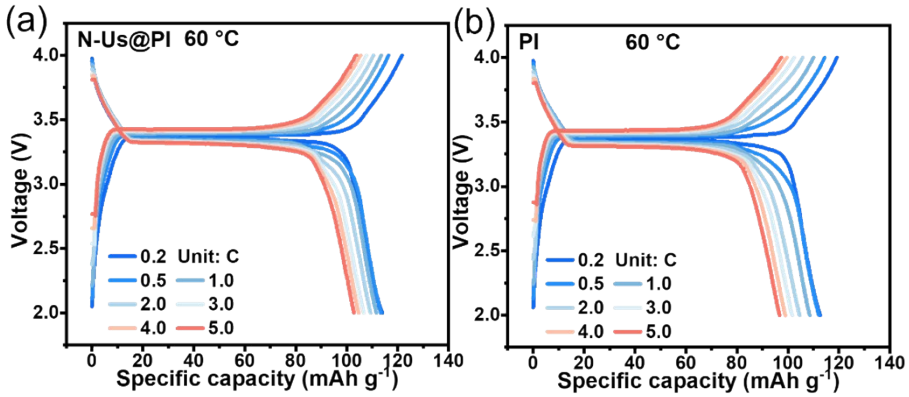

Fig. S18. GCD profiles of Na||NVP batteries employing different separators at 60 °C under various current rates: (a) Na|N-Us@PI|NVP, and (b) Na|PI|NVP.

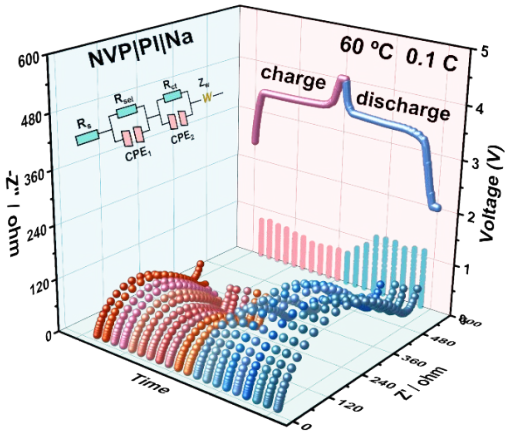

Fig. S19. *In-situ* EIS of Na|PI|NVP batteries at 60 °C and 0.1 C.

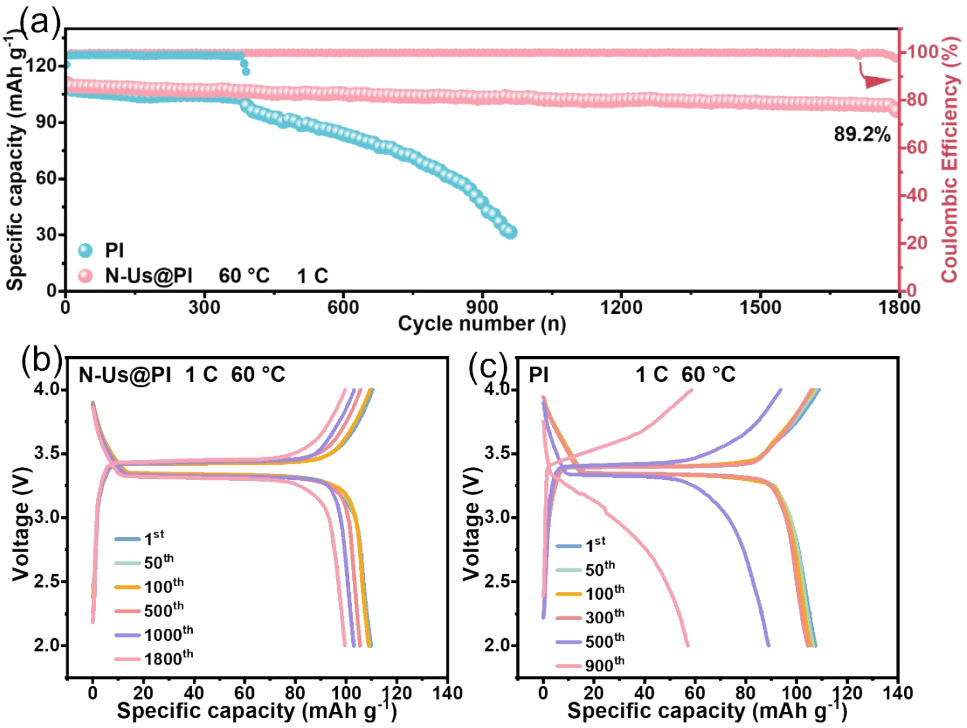

Fig. S20. The cycling stability of Na||NVP batteries employing different separators at 60 °C and 1 C: (a) cycling performance; GCD of (b) Na|N-Us@PI|NVP and (c) Na|PI|NVP.

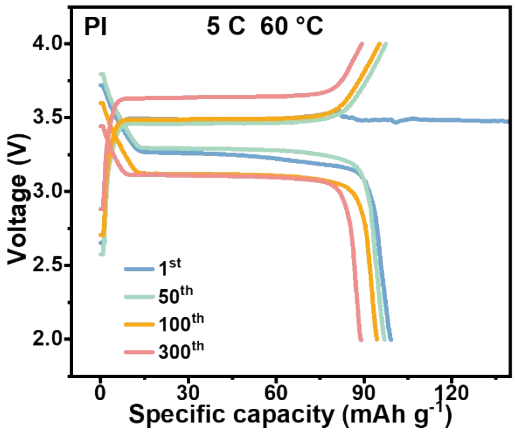

Fig. S21. GCD profiles of Na|PI|NVP batteries at 60 °C and 5 C.

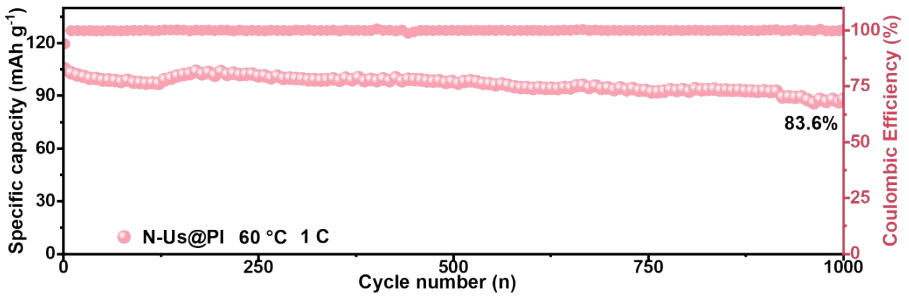

Fig. S22. Cycle performance of Na|N-Us@PI|NVP pouch cells at 60 °C and 1 C.